Mechanical and Finite Element Analysis of a Tree Microstructural Model Derived from Softwood Annual Rings

Yasin Furkan Gorgulu ,* and Murat Aydin

*Corresponding author: yasingorgulu@isparta.edu.tr

DOI: 10.15376/biores.20.3.7842-7855

GRAPHICAL ABSTRACT

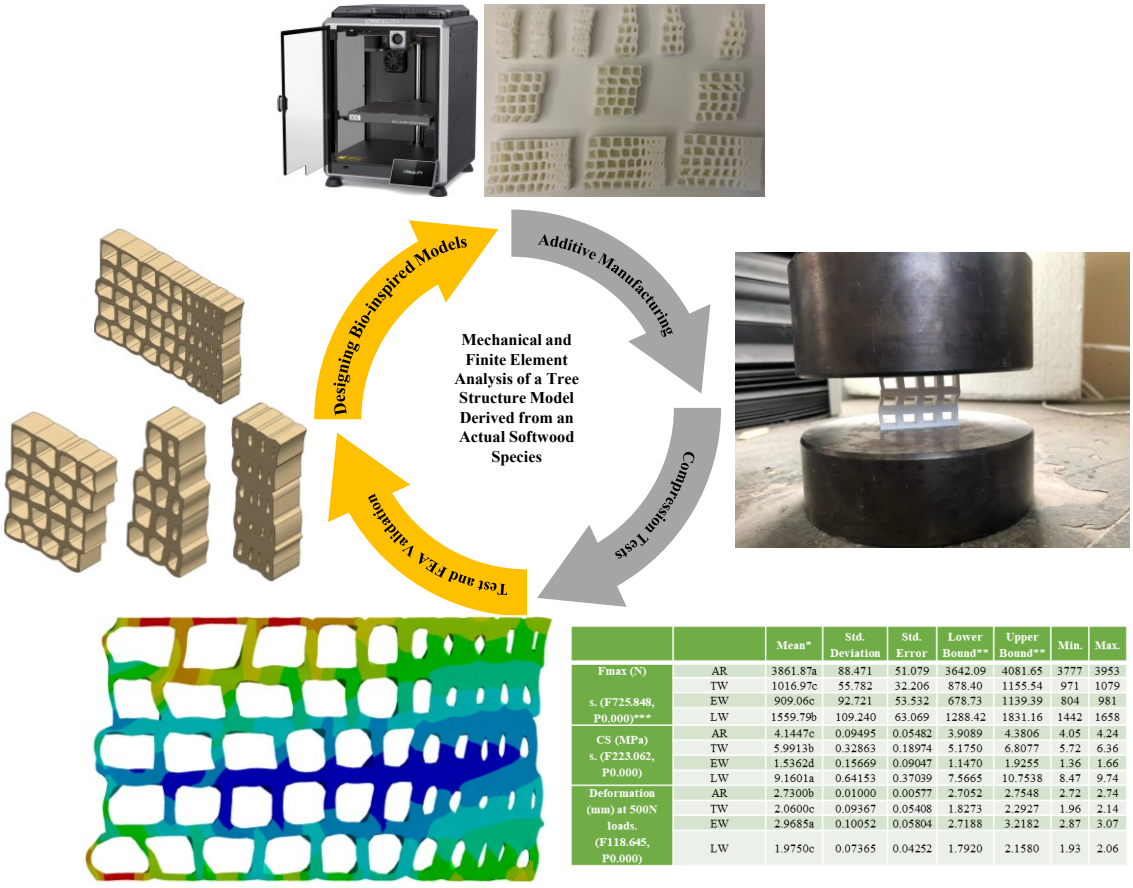

		Mean*	Std. Deviation	Std. Error	Lower Bound**	Upper Bound**	Min.	Max.
Fmax (N) s. (F725.848, P0.000)***	AR	3861.87a	88.471	51.079	3642.09	4081.65	3777	3953
	TW	1016.97c	55.782	32.206	878.40	1155.54	971	1079
	EW	909.06c	92.721	53.532	678.73	1139.39	804	981
	LW	1559.79b	109.240	63.069	1288.42	1831.16	1442	1658
CS (MPa) s. (F223.062, P0.000)	AR	4.1447c	0.09495	0.05482	3.9089	4.3806	4.05	4.24
	TW	5.9913b	0.32863	0.18974	5.1750	6.8077	5.72	6.36
	EW	1.5362d	0.15669	0.09047	1.1470	1.9255	1.36	1.66
	LW	9.1601a	0.64153	0.37039	7.5665	10.7538	8.47	9.74
Deformation (mm) at 500N loads. (F118.645, P0.000)	AR	2.7300b	0.01000	0.00577	2.7052	2.7548	2.72	2.74
	TW	2.0600c	0.09367	0.05408	1.8273	2.2927	1.96	2.14
	EW	2.9685a	0.10052	0.05804	2.7188	3.2182	2.87	3.07
	LW	1.9750c	0.07365	0.04252	1.7920	2.1580	1.93	2.06

Mechanical and Finite Element Analysis of a Tree Microstructural Model Derived from Softwood Annual Rings

Yasin Furkan Gorgulu ,* and Murat Aydin

A Scotch pine wood annual ring (AR) structure was modeled using AutoCAD and SolidWorks software. The same AR was separately modeled to create earlywood (EW), transition wood (TW), and latewood (LW). All 3D models were additively manufactured using Hyper PLA material and Creality 3D printer. Compression tests were performed to obtain load-deformation curves. The maximum force, compression strength (CS), and deformation at 500N load were determined. The EW presented the highest deformation while LW presented the highest CS. The TW and AR displayed intermediate behaviors. Finite Element Modeling and Analysis (FEM&A) was performed to compare with the experimental results. The numerical results presented considerable high deviations from the experiment. Around 78.7%, 41.7%, 89.3%, and 52% differences were observed for AR, EW, TW, and LW, respectively. Therefore, the capability of the model for prediction of mechanical behavior was not found to be successful. The essential reason for these discrepancies is the contrast between the orthotropic nature of wood and partially anisotropic nature of 3D printed models even if the filament is isotropic material. However, it should be taken into consideration that such high differences are not abnormal for the wood material even if the tested samples belong to the same log because of the variations in the material due to sampling details such as cutting location, orientation, *etc*. Furthermore, when considering the 3D printing parameters such as infill density, printing orientation, layer height, *etc.*, the FEM&A results can be considered partially successful, although the differences were high.

DOI: 10.15376/biores.20.3.7842-7855

Keywords: 3D printing; Compression testing; FEA; Hyper PLA material; Structural analysis

Contact information: Department of Machinery and Metal Technologies, Keciborlu Vocational School, Isparta University of Applied Sciences, Isparta, Turkiye;
** Corresponding author: yasingorgulu@isparta.edu.tr*

INTRODUCTION

The annual ring (AR) is one of the basic characteristics of wood. The structure of AR generally consists of three sections from the pith to bark which present the growth direction: earlywood (EW), transition wood (TW), and latewood (LW). These sequentially arrayed cells define both physical and mechanical properties of wood and all species differ from each other. Furthermore, the same species present different characteristics, which are formed by external factors. Environmental factors such as climate including precipitation, temperature, moisture, *etc*., are some of the essential influencing parameters of wood structure and consequently the AR features.

The influence of AR microstructure on physical and mechanical properties of wood is the critical area of interest in wood science and technology field. The following are some recent studies dealt with this issue. Lin *et al*. (2007) evaluated ring related compression strength of Taiwan incense cedar (*Calocedrus formosana*), Taiwan red cypress (*Chamaecyparis formosensis*), Japanese cedar (*Cryptomeria japonica*), Luanta fir (*Cunninghamia konishii*), China fir (*Cunninghamia lanceolata*), Taiwania (*Taiwania cryptomerioides*), and Chinese hemlock (*Tsuga chinensis*). Büyüksarı *et al*. (2017) determined the tensile strength of EW and LW of Scots pine and stated that LW values is 3.2 times higher than EW values. Roszyk *et al*. (2013) determined the tensile properties of EW and LW of Scots pine. Aydın and Yılmaz Adın (2023) evaluated the effect of AR number and width on the elastic constants of poplar. Aydın (2022) figured out the effect of AR number and width on ultrasonic wave velocity in pine (black, red, and Scots) and cedar woods. Interaction between the AR and bending properties are well determined, while compressive strength is not well established (Lin *et al.* 2007). Furthermore, calculating the specific features of EW, LW, and transition zones are difficult not only for sample preparation but also require advanced tools.

Nowadays, additive manufacturing (AM), is one of the advanced manufacturing technologies, which provides some advantages and has potential to replicate natural structures. Due to the versatility, researchers in wood science and technology field have focused on AM in different aspects such as preparing new wood-based filaments (Pringle *et al.* 2018), and furniture design or joint production (Aydın 2015; Yılmaz Aydın 2022; Demirel *et al*. 2024), biomimetic wood structure (Aydin and Yilmaz Aydin 2022; Aydın 2024; Aydın and Görgülü 2024), and tensile behavior (Bhagia *et al.* 2020; Eslami *et al.* 2021).

Wood has an orthotropic nature, which makes it difficult to determine its mechanical properties when compared to isotropic materials such as metals or acrylonitrile butadiene styrene (ABS) and polylactic acid (PLA), which are commonly used polymeric materials for fused filament fabrication in AM. However, 3D printing, a technique in AM, also provides some anisotropy to the structure due to production parameters such as infill density, printing orientation, patterns, layer height, raster angle, *etc.* Therefore, a partial resemblance between the 3D printed solid models and wood structure may be established. This limited resemblance may provide some comparison opportunity for the mechanical behavior of wood. On the other hand, it is also known that micro-structure of wood cannot be printed using the 3D printing technology in use. Furthermore, it is also doubtful that the structures and parts that can replace the wooden material can be economically obtained by three-dimensional printing. However, such studies may have laid a stone in the direction of achieving some improvement in this challenge. Therefore, in this study, the primary objective was to investigate the mechanical behavior of AR, EW, TW, and LW geometries under compression. To achieve this, advanced techniques such as 3D printing and Finite Element Analysis (FEA) were employed. The rationale behind using 3D printing was to create precise, scalable models of complex wood structures, allowing for accurate physical testing. Hyper PLA material and the Creality K1C printer enable the production of detailed and consistent samples. The application of FEA, specifically using ANSYS static structural analysis, allows for the simulation of compression tests, providing a comprehensive understanding of the stress distribution and deformation characteristics of the geometries. By comparing the experimental results with FEA simulations, it was aimed to validate the reliability of the computational models, which can significantly reduce the need for

extensive physical testing and accelerate the development of new materials and structures with optimized mechanical properties. This approach not only enhances the accuracy of the analysis, but it also offers a cost-effective and time-efficient method for studying the structural behavior of wood under various loading conditions. Due to uniqueness of the wood structure, it is not easy to model a realistic microstructure of wood. Therefore, an actual well-presented cross-section of a wood was chosen from the study written by Arzac *et al.* (2018) and Reed and Lidestav (2023). The cross-section of an AR belongs to Scotch pine, presented in Fig. 1, was based on performing this study.

MATERIALS AND METHODS

The annual ring structure of *Pinus sylvestris* was replicated using SolidWorks, based on the geometries described in Arzac *et al.* (2018). Four different three-dimensional (3D) solid models were created: one complete annual ring, early wood, transition wood, and latewood sections. The dimensions and structural details of these geometries were adapted and scaled according to the specifications provided in the original study. For instance, the width of the annual ring was scaled to 73.2 mm, height to 48.37 mm, and extruded by 10 mm. Fused Deposition Modeling (FDM) was used for AM. The polylactic acid (PLA) filament was used for layer accumulation. The Creality K1C device was used for three-dimensional (3D) printing. The parameters used for manufacturing is presented in Table 1. The standard triangle language (STL) files of the models were created and prepared for 3D printing using fused deposition modeling. The detailed dimensions and scaling factors are provided in Table 1 of Arzac *et al.* (2018).

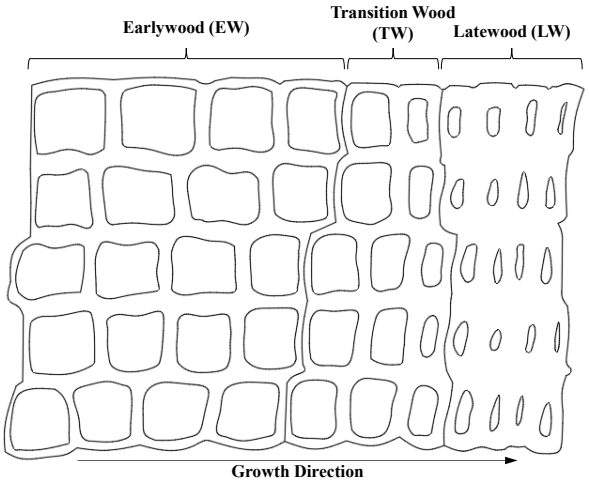

Fig. 1. Annual ring structure for modeling and additive manufacturing (Arzac *et al.* 2018; Reed and Lidestav 2023)

Additive Manufacturing

In this study, the different wood geometries were fabricated using additive manufacturing techniques. The parts were printed using a Creality K1C 3D printer with Creality Print slicing software. Hyper PLA was selected as the material for 3D printing due to its superior mechanical properties compared to traditional ABS (Acrylonitrile Butadiene Styrene). According to data provided by Creality, Hyper PLA exhibits a tensile strength of 53.0 MPa and a bending strength of 92.4 MPa. In contrast, ABS has a tensile

strength of 46 MPa and a bending strength of 68 MPa (Creality 2024). These enhanced properties of Hyper PLA make it an ideal choice for creating robust and reliable models for mechanical testing, ensuring that the printed samples can withstand the stress and strain applied during the compression tests and provide accurate and consistent results for comparison with FEA simulations. Specimens printed with additive manufacturing are given in Fig. 2.

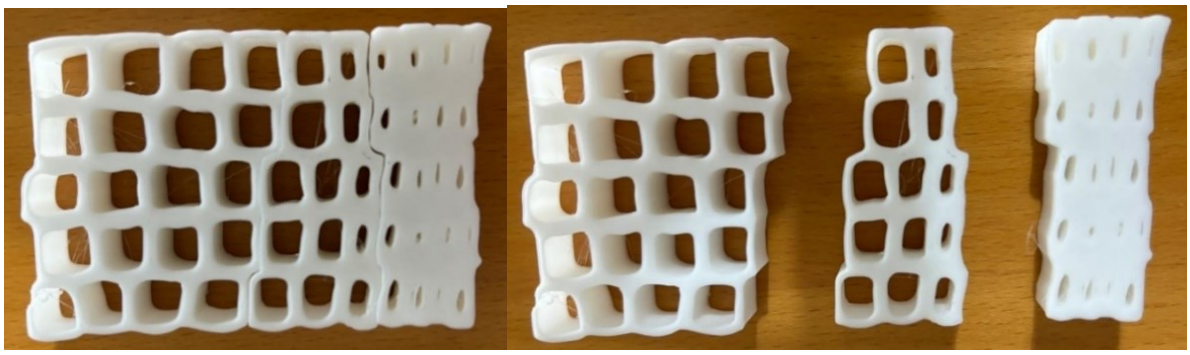

Fig. 2. Additively manufactured parts forming an annual ring composition

Table 1. Properties of Hyper PLA filament

Density (kg/m³)	Diameter (mm)	Color	Thermal Properties - Temperature (°C)	
			Printing	Hot Bed
1.25	1.75±0.03	White	190-230	25-60

Compression Test

Compression tests were performed to obtain load-deformation curves. The universal test machine (Marestek, İstanbul, Türkiye) was used for destructive test. The load was applied corresponding to the tangential (T) direction of wood. Therefore, T direction compression strength (CS) of the *Pinus sylvestris* was taken into consideration for discussion. To prevent slantwise deformation, samples were fixed on the compression and load cell fixtures using double sided tape. Due to layer accumulation limited slantwise-like deformation was observed due to spring-back behavior of the samples.

ASTM D695 (2015) or ISO 604 (2002) presents the details for compression properties of the rigid plastics. Therefore, the compression test (CT) was performed 1.6 mm/min loading speed. The maximum force (N), the strength CS, and deformation (mm) at 500 N load were determined for each model. The Eq.1 was used for CS calculation,

$$\mathrm{CS} = \frac{F_{max}}{A} \quad (1)$$

where CS is the compression strength (MPa), $F_{\max}$ is the maximum load, and A is the area (mm²) of the sample.

The compression behavior of bio-inspired AM models was also numerically simulated using ANSYS and compared to static test results. The details of the finite element models are presented in Fig. 3 and Table 2.

The one-way ANOVA test was performed to compare the means. The Duncan multiple range test was conducted as post-hoc to figure out the statistically significant differences in the means.

Finite Element Analysis

Finite Element Analysis was conducted using ANSYS static structural analysis to simulate the compression tests of the different wood geometries, EW, TW, LW, and the complete AR. The 3D models created in SolidWorks were imported into ANSYS for meshing and analysis. Each model was meshed using tetrahedral elements, with the mesh density adjusted to ensure accurate results while maintaining computational efficiency. The mechanical properties of Hyper PLA, including a tensile modulus of 1150 MPa, tensile strength of 53.0 MPa, bending strength of 92.4 MPa, flexural modulus of 2490 MPa, and Poisson's ratio of 0.33, were assigned to the models (Table 2). These values provide for numerical models that are inherently isotropic at a microscopic level. However, due to the cellular structure of the model, the larger-scale effect is to emulate an anisotropic structure formation, even if the PLA is an isotropic material. Therefore, this is the main limitation of the study, and the essential factor for the possible diffraction in mechanical behavior. Boundary conditions were applied by fixing the bottom surface of each model and applying a uniform displacement of 6 mm on the top surface to mimic the compression test conditions.

Table 2. Properties of Plastic, Hyper PLA used in the Analyses

Plastic, Hyper PLA	
Density	1.25 g/cm^3
Tensile Modulus (X-Y)	1146.064
Tensile Strength (X-Y)	52.991 MPa
Bending Strength (X-Y)	92.381 MPa
Flexural Modulus (X-Y)	2490.178 MPa
Poisson's Ratio	0.33

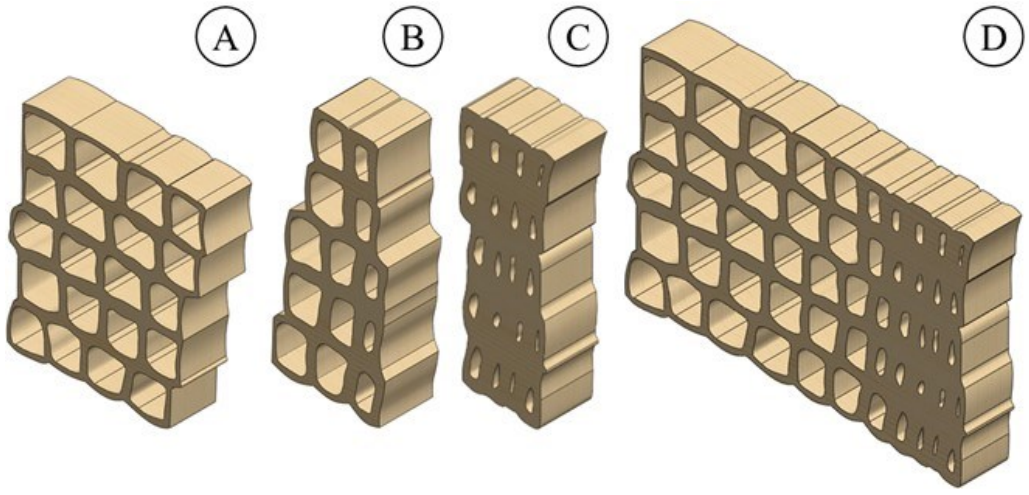

Fig. 3. Solid models of the specimens; A: EW, B: TW, C: LW, and D: AR

The resulting stress and strain distributions were calculated and compared to the experimental results to validate the accuracy of the FEA simulations. Figure 3 illustrates the different geometries analyzed, highlighting the specific regions of early wood,

transition wood, latewood, and the annual ring. Mesh structures of the four geometries are also depicted in Fig. 4.

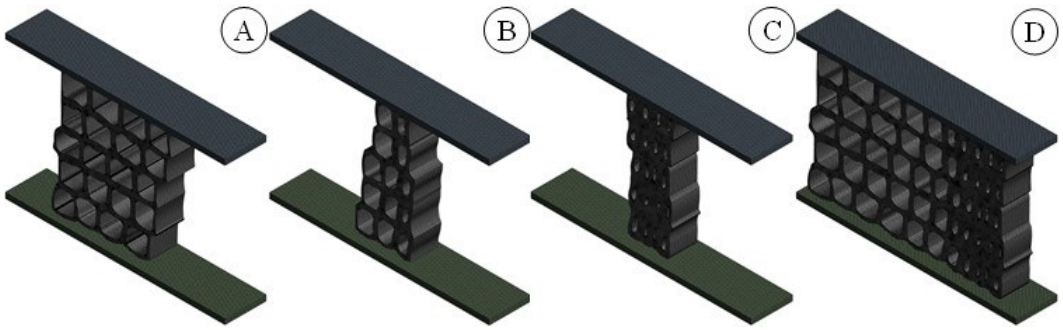

Fig. 4. Mesh structures of the specimens; A: EW, B: TW, C: LW, and D: AR

To maintain consistency, the mesh size was kept uniform across all four geometries. The mesh metrics, including the number of nodes, elements, average skewness, and orthogonal quality, are detailed in Table 3., ensuring that the mesh quality was sufficient for accurate simulation results.

Table 3. Mesh Metrics Table

Specimen	Nodes	Elements	Average Skewness	Skewness Status	Average Orthogonal Quality	Orthogonal Quality Status
AR	941,400	201,680	0.16359	Excellent	0.95752	Excellent
EW	550,749	113,720	0.13766	Excellent	0.96467	Excellent
TW	364,064	75,240	0.09810	Excellent	0.96949	Excellent
LW	483,657	104,560	0.13083	Excellent	0.95661	Excellent

To analyze the mechanical properties of cell walls during compression, stress, and strain are determined by the following equations (Cambaz *et al.* 2022; Yan *et al.* 2022),

$$\sigma_{nom} = \frac{F}{A} \tag{2}$$

$$\varepsilon_{nom} = \frac{d_y}{H} \tag{3}$$

where σ_{nom} is nominal stress (MPa); F denotes the contact force between pressure plates (N), A is the initial contact area between pressure plates (mm^2), ε_{nom} is nominal strain (mm/mm), d_y denotes displacement (mm), and H is initial height of the specimen (mm) Von-Mises stress, also known as effective stress, can be expressed as,

$$\sigma_{vm} = \sqrt{0.5[(\sigma_x - \sigma_y)^2 + (\sigma_y - \sigma_z)^2 + (\sigma_z - \sigma_x)^2] + 3(\tau_{xy}{}^2 + \tau_{yz}{}^2 + \tau_{zx}{}^2)} \tag{4}$$

where: σ_x, σ_y, and σ_z are the normal stresses (MPa), and τ_{xy}, τ_{yz}, and τ_{zx} are the shear stresses (MPa) in the three orthogonal directions.

RESULTS AND DISCUSSION

Compression Test Results

The average values and statistics for the compression properties of samples are presented in Table 4. The maximum force for the AR, TW, EW, and LW ranged from 3780 to 3950 N, 971 to 1080 N, 804 to 981 N, and 1440 to 1680 N, respectively. The CS ranges were 4.05 to 4.24 MPa, 5.72 to 6.36 MPa, 1.36 to 1.66 MPa, and 8.47 to 9.74 MPa, respectively. The deformation values ranges were 2.72 to 2.74 mm, 1.96 to 2.14 mm, 2.87 to 3.07 mm, and 1.93 to 2.06 mm, respectively. ANOVA results demonstrated that mechanical behavior of 3D printed models of the real wood structures presented statistically significant differences. As can be seen in Fig. 2, the size, shape, and intensity of the material of the models were remarkably different, which can be assumed the essential reason for the significant deviations. Furthermore, distinctive differences in the cell formation were responsible for such diffractions when comparing the sections of AR. Early wood demonstrated lower stress resistance and higher strain values indicative of its softer, less dense nature. In contrast, the LW showed higher stress resistance and lower strain values reflecting its denser, stronger composition. The transition region and annual ring presented intermediate behaviors aligning with their composite structures. Standalone, F_{max} average for AR was around 2.5 times higher than LW. However, CS of AR around was ½ of LW. Besides being attributable to its solid state (being denser), surface area is the key multiplying factor for obtaining such opposite results. Furthermore, as Zhao *et al*. (2024) noticed, size of the specimen also has an influence on CS.

Table 4. Compression Test Results for Different Wood Geometries

		Mean*	Std. Deviation	Std. Error	Lower Bound**	Upper Bound**	Min.	Max.
F_{max} (N) s. (F725.848, P(0.000)* **	**AR**	3861.87a	88.471	51.079	3642.09	4081.65	3777	3953
	TW	1016.97c	55.782	32.206	878.40	1155.54	971	1079
	EW	909.06c	92.721	53.532	678.73	1139.39	804	981
	LW	1559.79b	109.240	63.069	1288.42	1831.16	1442	1658
CS (MPa) s. (F223.062, P(0.000)	**AR**	4.1447c	0.09495	0.05482	3.9089	4.3806	4.05	4.24
	TW	5.9913b	0.32863	0.18974	5.1750	6.8077	5.72	6.36
	EW	1.5362d	0.15669	0.09047	1.1470	1.9255	1.36	1.66
	LW	9.1601a	0.64153	0.37039	7.5665	10.7538	8.47	9.74
Deformation (mm) at 500N load s. (F118.645, P(0.000)	**AR**	2.7300b	0.01000	0.00577	2.7052	2.7548	2.72	2.74
	TW	2.0600c	0.09367	0.05408	1.8273	2.2927	1.96	2.14
	EW	2.9685a	0.10052	0.05804	2.7188	3.2182	2.87	3.07
	LW	1.9750c	0.07365	0.04252	1.7920	2.1580	1.93	2.06

*Duncan's homogeneity groups, **95% Confidence Interval for Mean, and *** ANOVA results. Significant.

In the literature, there has been scarcely any study that provided mechanical behavior of additively manufactured real wood structure. Therefore, a comparison and discussion can be done over a few related studies as follows. Lin *et al*. (2007) reported 3 to 10.4 MPa tangential CS for seven softwood species grown in Taiwan. When considering the experimental value, the CS of this study corresponds to tangential direction and are in agreement with the reported range. Mańkowski and Laskowska

(2021) reported the CS of LW (parallel to the grain) from yellow pine, which is around 2.5 times higher than EW. Lin and Chiu (2007) expressed that CS (parallel to the grain) increases with decrease in LW and EW. In this study, CS of LW is around 6 times higher than EW. The order of the compressive stress for Douglas fir is LW > AR > EW (Wang et al. 2023) as found in this study. This is because of the thin cell walls and large cell lumens; the EW was easy to compress. This simple and basic interaction can be observed over the deformation styles of the models presented in Fig. 5.

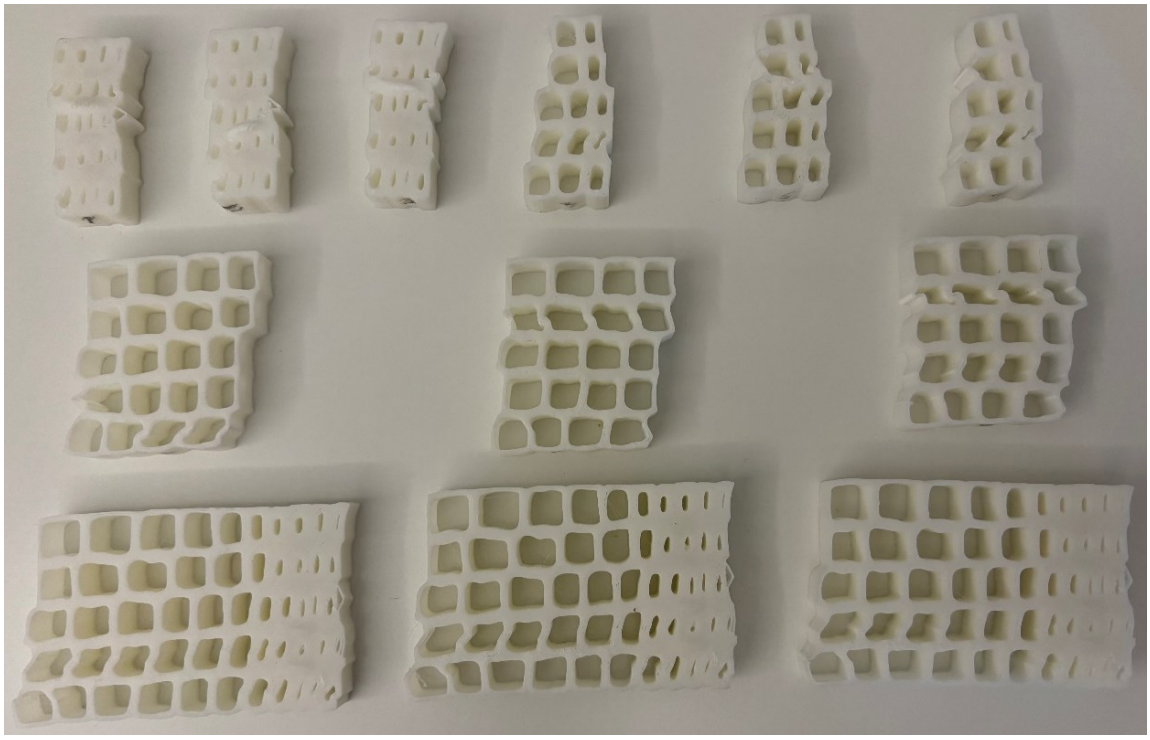

Fig. 5. Deformation of the 3D printed models

Mańkowski and Laskowska (2021) reported that the CS of LW is twice as high as the CS of LW for Scots pine. The CS mean for EW is around 33 MPa while LW is around 65 MPa. In this study, CS of EW and LW were found to be 1.5 MPa and 9.2 MPa, respectively. Therefore, the value of around 6 times higher LW is not in harmony with the literature. This can be associated with basic diffraction between the structure of the 3D printed samples and wood.

Krauss *et al*. (2011) reported that modulus of elasticity (MOE) values of EW are lower than LW for the Scotch pine. Similarly, Büyüksari *et al.* (2017) reported 37.3 MPa and 93.9 MPa bending strength and 1.56 MPa and 3.6 MPa MOE for EW and LW of Scotch pine, respectively. Therefore, cell walls are one of the basic factors for the determination of strength. On the other hand, it cannot be expected that partially anisotropic nature of 3D printed samples presents harmony with the actual wood mechanical properties.

Finite Element Analysis Results

In this study, four distinct geometries representing different wood regions were analyzed: macroscopic magnified EW, TW, LW, and AR combining these three regions. Each sample underwent a compression test both in the laboratory and through ANSYS

static structural analysis. The compression tests involved applying a total displacement of 6 mm using compression plates at the top and bottom surfaces of the samples. The resulting deformation, strain, and stress contours from the ANSYS simulations are illustrated in Figs. 4 to 6.

As shown in Fig. 6., the EW region exhibited the highest deformation values among the four samples. This is expected due to the less dense and more porous structure of EW, which allows for greater deformation under compressive loads. The strain analysis (Fig. 7) showed high strain concentrations, indicating significant deformation behavior. The stress analysis (Fig. 8.) demonstrated areas of high stress concentration, particularly near the points of contact with the compression plates. The transition region displayed moderate deformation levels. This region serves as an intermediate phase between EW and LW, reflecting a gradual increase in density and mechanical strength. The strain distribution highlighted areas of moderate strain, consistent with its transitional nature. The stress distribution indicated significant stress in regions transitioning between different wood structures.

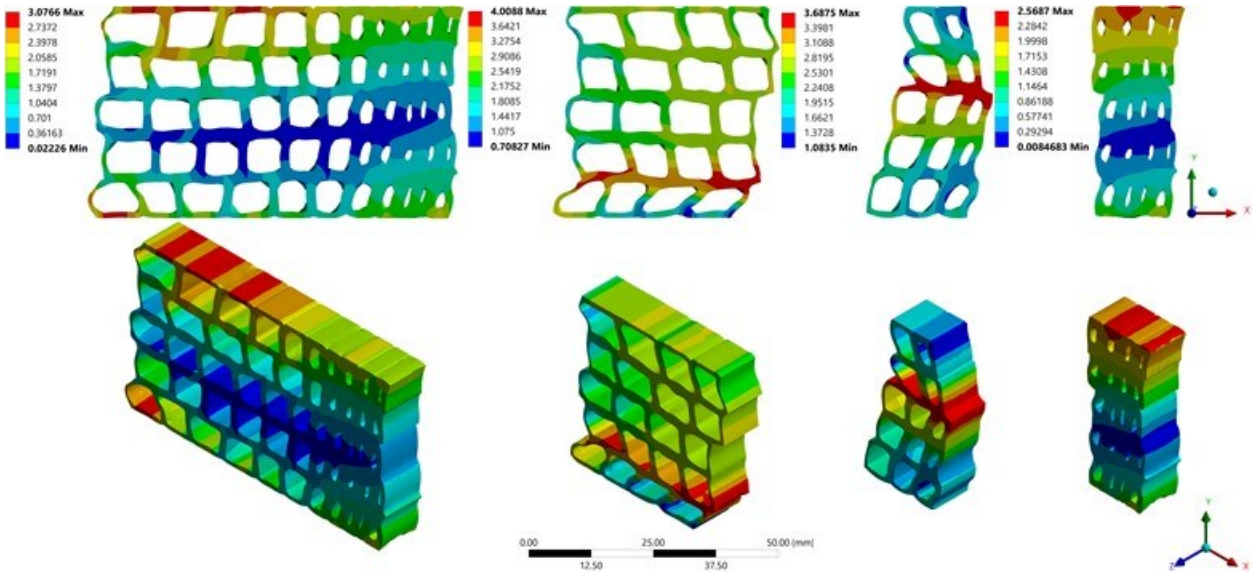

Fig. 6. Deformation contours of the four geometries

The latewood region exhibited the lowest deformation values. The dense and compact structure of LW contributed to its higher resistance to compressive forces. The strain analysis revealed lower strain values, indicating higher structural rigidity. The stress analysis shows high stress concentrations, which is indicative of the material's resistance to deformation under load.

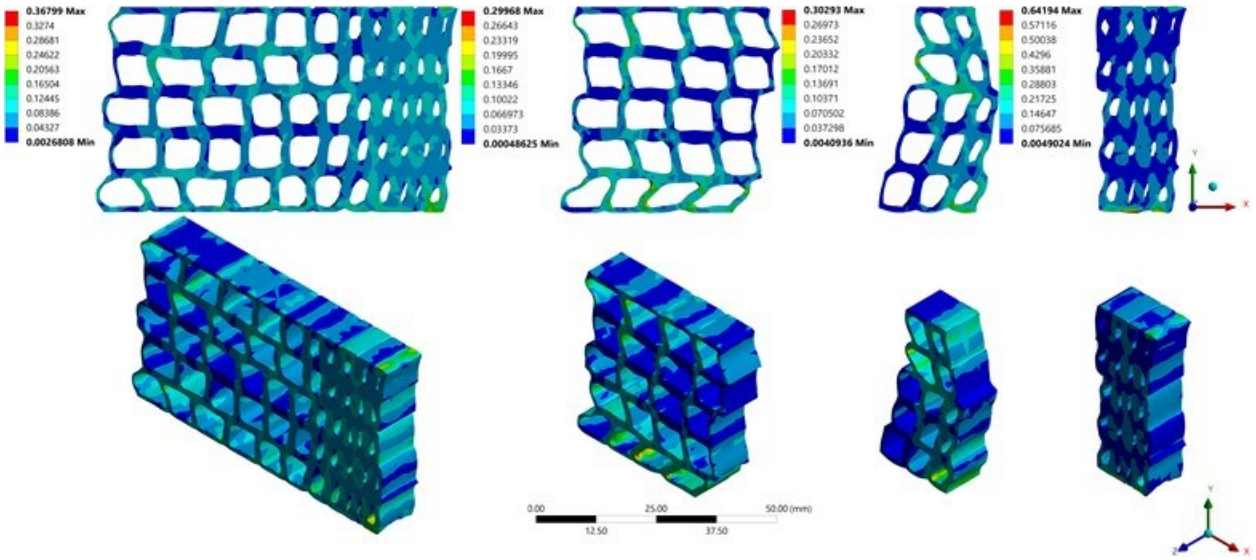

Fig. 7. Strain contours of the four geometries

The annual rings showed a combination of deformation characteristics from all three regions. The contour plot indicates varying deformation levels corresponding to the distinct properties of EW, transition region, and LW within the annual ring structure. The strain shows a mix of strain concentrations reflecting the composite nature of this geometry. The stress analysis indicates a complex stress distribution pattern due to the combined characteristics of the constituent regions.

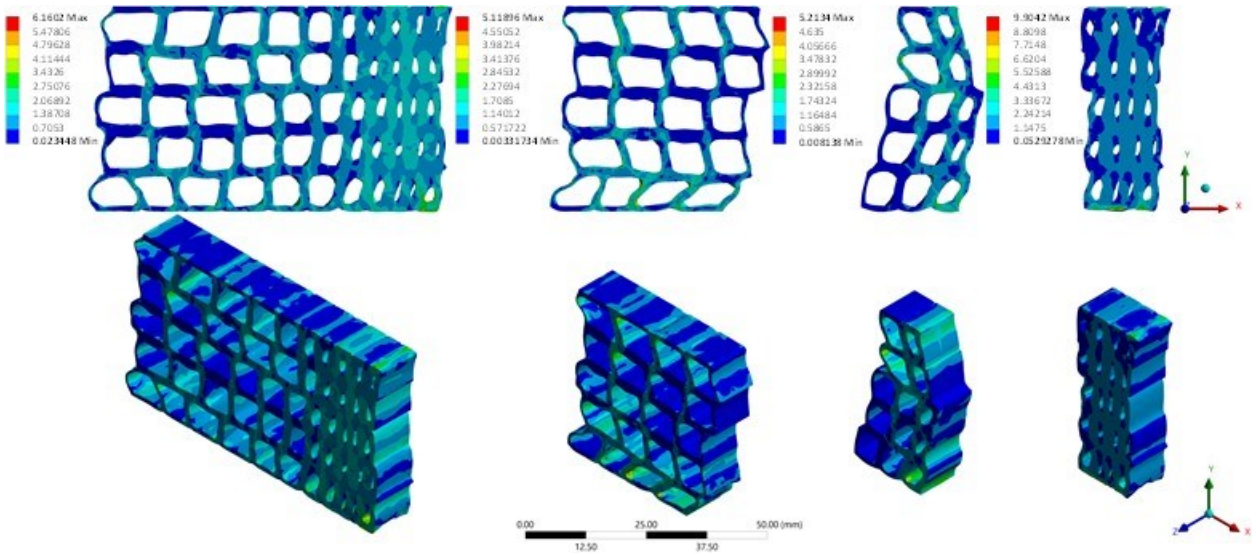

Fig. 8. Stress contours of the four geometries

The laboratory compression tests corroborated the simulation findings, with EW exhibiting the greatest deformation and LW the least. The transition region displayed intermediate behavior, and the annual ring's deformation pattern mirrored the combined characteristics of its constituent regions.

Further analysis of the stress-strain curves obtained from both the laboratory tests and ANSYS simulations revealed consistent trends. Early wood demonstrated lower stress resistance and higher strain values, indicative of its softer, less dense nature. In

contrast, LW showed higher stress resistance and lower strain values, reflecting its denser, stronger composition. The transition region and AR presented intermediate behaviors, aligning with their composite structures.

Numerous studies have explored the mechanical properties of wood-polymer composites and 3D-printed materials using FEA and various experimental techniques. A study on wood-polymer composites produced *via* fused deposition (FDM) modeling demonstrated that numerical homogenization could effectively predict the mechanical behavior of these composites, with a relative error between numerical results and experimental data not exceeding 10% (Ezzaraa *et al*. 2023). Research on wood fiber/PLA composites printed at different speeds found that higher printing speeds negatively impacted the CS values and modulus, with a decrease in printing speed from 70 mm/s to 30 mm/s resulting in a 34.3% decrease in CS (Yang and Yeh 2020). Another study investigating the tensile and flexural properties of wood/PLA composites showed that the addition of wood sawdust improved mechanical properties, particularly tensile strength and flexural modulus (Narlıoğlu *et al.* 2021). Additionally, a nonlinear FEA study simulating the uniaxial tensile behavior of 3D-printed PLA parts revealed that the maximum deviation between experimental and simulated results was only 6.7%, indicating the accuracy of FEA in predicting mechanical behavior under tensile loads (Alharbi *et al.* 2020). Case studies from the Oslo School of Architecture and Design highlighted the integration of FEA in the design and analysis of 3D-printed materials, demonstrating how FEA can optimize material distribution and structural integrity (Killi and Morrison 2016) .

These findings described above align closely with this study, which employed both experimental compression tests and FEA to analyze the mechanical behavior of different wood geometries. The percentage differences between the present laboratory measurements and FEA results—78.69% for the AR, 41.73% for EW, 89.31% for TW, and 52.01% for LW—reflect the limitations of simulating the complex, anisotropic nature of natural wood using isotropic 3D-printed materials. Nevertheless, the trends observed in the deformation and stress distribution patterns show reasonable consistency between the experimental and numerical results. These findings support the utility of FEA in capturing the general mechanical behavior of bio-inspired geometries, particularly when combined with experimental validation.

Overall, the ANSYS static structural analysis effectively captured the mechanical behavior of the different wood regions under compression. The simulation results provide valuable insights into the structural integrity and deformation characteristics of wood, aiding in the design and application of wood-based materials in engineering and construction. The findings of this study pave the way for future research and applications in material science and engineering, particularly in the development of new wood-based materials and the optimization of their mechanical properties through advanced modeling techniques.

CONCLUSIONS

This study successfully demonstrated the mechanical behavior of different wood geometries under compression using both experimental tests and finite element analysis (FEA) simulations.

The results indicated that earlywood (EW) exhibited the highest deformation, reflecting its less dense and more porous structure, while latewood (LW) displayed the lowest deformation, confirming its denser and more robust nature. Specifically, the experimental compression tests revealed that EW had the highest deformation values, whereas LW had the highest compression strength and the lowest deformation.

The actual experimental and numerical wood-based models presented considerable diffractions in terms of stress and strain. For example, the diffraction between compression test (CT) and finite element analysis (FEA) results were around 78.7% for AR, 41.7% for EW, 89.3% for TW, and 52% for LW. Such significant differences can be attributed to the 3D printing parameters, which form the part structure. Therefore, infill density and pattern, shell thickness, layer height and orientation, nozzle diameter, fill orientation or angle, filament properties *etc.* may cause such diffractions. Due to the complex polar orthotropic nature of wood, it is not easy to biomimicry the exact micro-structure. Therefore, although it seems high, such differences can be acceptable when considering the diffraction of physical and mechanical properties of wood samples even if prepared from the same log and or same cutting location.

ACKNOWLEDGMENTS

The authors declare that they have no conflict of interest. Additionally, the research presented in the manuscript did not receive any external funding. The authors would like to thank the Department of Machinery and Metal Technologies and Civil Engineering. The raw/processed data required to reproduce these findings cannot be shared at this time as the data also forms part of an ongoing study.

REFERENCES CITED

Alharbi, M., Kong, I., and Patel, V. I. (2020). "Simulation of uniaxial stress–strain response of 3D-printed polylactic acid by nonlinear finite element analysis," *Applied Adhesion Science* 8(1), 5. DOI: 10.1186/s40563-020-00128-1

Arzac, A., Babushkina, E. A., Fonti, P., Slobodchikova, V., Sviderskaya, I. V., and Vaganov, E. A. (2018). "Evidences of wider latewood in *Pinus sylvestris* from a forest-steppe of Southern Siberia," *Dendrochronologia* 49(November 2017), 1-8. DOI: 10.1016/j.dendro.2018.02.007

ASTM D695. (2015). "Standard test method for compressive properties of rigid plastics," <https://www.astm.org/d0695-15.html?a=> (Nov. 19, 2022).

Aydın, M. (2015). "Additive manufacturing: Is it a new era for furniture production?" *Journal of Mechanics Engineering and Automation 5*(6), 338-347. DOI: 10.17265/2159-5275/2015.06.002

Aydın, M. (2022). "Effects of annual ring number and width on ultrasonic waves in some softwood species," *BioResources* 17(1), 1745-1763. DOI: 10.15376/biores.17.1.1745-1763

Aydin, M., and Yilmaz Aydin, T. (2022). "Bio-mimicry: Tree rings and three-dimensional printing – Preliminary biomimetic experiments with fused deposition modeling using acrylonitrile butadiene styrene filament," *BioResources* 17(4), 6588-6597. DOI: 10.15376/biores.17.4.6588-6597

Aydın, M., and Aydın, T. Y. (2023). "Influence of growth ring number and width on elastic constants of poplar," *BioResources* 18(4), 8484-8502. DOI: 10.15376/biores.18.4.8484-8502

Aydın, M. (2024). "Compression behavior of the wood-inspired cellular structure of acrylonitrile butadiene styrene," *Materials Testing* 66(1), 66-74. DOI: 10.1515/mt-2023-0147

Aydin, M., and Gorgulu, Y. F. (2024). "Structural investigation of wood-inspired cell wall geometries using additive manufacturing: Compression testing and finite element analysis validation," *BioResources* 19(4), 7493-7512. DOI: 10.15376/biores.19.4.7493-7512

Bhagia, S., Lowden, R. R., Erdman, D., Rodriguez, M., Haga, B. A., Solano, I. R. M., Gallego, N. C., Pu, Y., Muchero, W., Kunc, V., and Ragauskas, A. J. (2020). "Tensile properties of 3D-printed wood-filled PLA materials using poplar trees," *Applied Materials Today* 21, article 100832. DOI: 10.1016/j.apmt.2020.100832

Büyüksarı, Ü., As, N., and Dündar, T. (2017). "Mechanical properties of earlywood and latewood sections of scots pine wood," *BioResources* 12(2), 4004-4012. DOI: 10.15376/biores.12.2.4004-4012

Cambaz, A., Gorgulu, Y. F., and Arat, H. (2022). "Analysing fluid-structure interaction with CFD and FEA on a marine double-wall LNG piping system," *Multidisciplinary Scientific Journal of Maritime Research* 36(1), 51–60. DOI: 10.31217/p.36.1.6

Creality. (2024). "Creality Hyper 1.75mm PLA 3D Printing Filament," <https://www.creality3dofficial.eu/products/hyper-1.75mm-pla-3d-printing-filament> (May 31, 2024).

Demirel, S., Kuvel, N. T., Çava, K., and Aslan, M. (2024). "The performance of 3d printed dowel with three different surface designs in furniture joints," *Turkish Journal of Forestry | Türkiye Ormancılık Dergisi*, 100-106. DOI: 10.18182/tjf.1387389

Eslami, H., Jayasinghe, L. B., and Waldmann, D. (2021). "Nonlinear three-dimensional anisotropic material model for failure analysis of timber," *Engineering Failure Analysis* 130, article 105764. DOI: 10.1016/j.engfailanal.2021.105764

Ezzaraa, I., Ayrilmis, N., Abouelmajd, M., Kuzman, M. K., Bahlaoui, A., Arroub, I., Bengourram, J., Lagache, M., and Belhouideg, S. (2023). "Numerical modeling based on finite element analysis of 3D-printed wood-polylactic acid composites: A comparison with experimental data," *Forests* 14(1), article 95. DOI: 10.3390/f14010095

ISO 604. (2002). *Plastics — Determination of compressive properties*.

Killi, S., and Morrison, A. (2016). "FEA and 3D printing, the perfect match?," *International Journal of Mechanical Systems Engineering*, 2(1). DOI: 10.15344/2455-7412/2016/111

Krauss, A., Moliński, W., Kúdela, J., and Čunderlík, I. (2011). "Differences in the mechanical properties of earlyand latewood within individual annual rings in dominant pine tree (*Pinus sylvestris* L.)," *Wood Research* 56(1), 1-12.

Lin, C.-J., Tsai, M.-J., Lee, C.-J., Wang, S.-Y., and Lin, L.-D. (2007). "Effects of ring characteristics on the compressive strength and dynamic modulus of elasticity of seven softwood species," *Holzforschung* 61(4), 414-418. DOI: 10.1515/HF.2007.077

Mańkowski, P., and Laskowska, A. (2021). "Compressive strength parallel to grain of earlywood and latewood of yellow pine," *Maderas. Ciencia y Tecnología* 23. DOI: 10.4067/S0718-221X2021000100457

Narlıoğlu, N., Salan, T., and Alma, M. H. (2021). "Properties of 3D-printed wood sawdust-reinforced PLA composites," *BioResources* 16(3), 5467-5480. DOI: 10.15376/biores.16.3.5467-5480

Pringle, A. M., Rudnicki, M., and Pearce, J. M. (2018). "Wood furniture waste–based recycled 3-D printing filament," *Forest Products Journal* 68(1), 86-95. DOI: 10.13073/FPJ-D-17-00042

Reed, M. G., and Lidestav, G. (2023). "Boreal forests in the face of climate change," in: *Advances in Global Change Research*, M. M. Girona, H. Morin, S. Gauthier, and Y. Bergeron (eds.), Springer International Publishing, Cham. DOI: 10.1007/978-3-031-15988-6

Roszyk, E., Kwiatkowski, T., and Moliński, W. (2013). "Mechanical parameters of pine wood in individual annual rings under tensile stress along the grains in dry and wet state," *Wood Research* 58(4), 571-580.

Wang, J., Yang, K., Li, W., Wang, X., Van den Bulcke, J., and Van Acker, J. (2023). "The impact of earlywood and latewood on the compressive stress of thermally modified Douglas fir," *Forests* 14(7), article 1376. DOI: 10.3390/f14071376

Yan, S., Eichhorn, S. J., and Toumpanaki, E. (2022). "Numerical simulation of transverse compression and densification of wood," *Wood Science and Technology* 56(4), 1007-1027. DOI: 10.1007/s00226-022-01388-9

Yang, T.-C., and Yeh, C.-H. (2020). "Morphology and mechanical properties of 3D printed wood fiber/polylactic acid composite parts using fused deposition modeling (FDM): The effects of printing speed," *Polymers* 12(6), article 1334. DOI: 10.3390/polym12061334

Yılmaz Aydın, T. (2022). "Do it yourself furniture: Part A – Designing fittings for an easy to manufacture hybrid chair," *Mobilya ve Ahşap Malzeme Araştırmaları Dergisi* 5(1), 50-60. DOI: 10.33725/mamad.1129596

Article submitted: February 28, 2025; Peer review completed: May 17, 2025; Revised version received and accepted: June 5, 2025; Published: July 31, 2025.
DOI: 10.15376/biores.20.3.7842-7855